J Mater Sci (2021) 56:13499–13508

Ceramics

Effects of sintering method on the structural, dielectric and energy storage properties of $AgNbO_3$ lead-free antiferroelectric ceramics

Tianyu Li[1], Wenjun Cao[1], Pengfei Chen[1], Jinsong Wang[1], and Chunchang Wang[1,2,*]

[1] Laboratory of Dielectric Functional Materials, School of Physics & Materials Science, Anhui University, Hefei 230601, China
[2] State Key Laboratory of Low-Dimensional Quantum Physics, Department of Physics, Tsinghua University, Beijing 100084, China

Received: 8 March 2021
Accepted: 4 May 2021
Published online: 18 May 2021

ABSTRACT

In this work, we systematically investigated the effects of single-step and two-step sintering methods on the structural, dielectric and energy storage properties of pure $AgNbO_3$ lead-free antiferroelectric ceramics. Compared with the single-step sintered ceramic, the ceramic prepared by two-step sintering method has smaller grain size, dense and homogeneous microstructure. In addition, the results of dielectric temperature spectra reveal that the two-step sintering method hardly changes the phase transition temperature of $AgNbO_3$ ceramics but greatly decreases the dielectric loss value. Most importantly, the ceramic prepared by the two-step sintering method displays high breakdown electric field strength (22 kV/mm), larger recoverable energy storage density-W_{rec} (2.59 J/cm^3) and higher energy storage efficiency-η (45%) as well as excellent temperature stability than those of the ceramic by single-step sintering method. Furthermore, it also exhibited high power density (P_D = 25.7 MW/cm^3) and extremely fast charge–discharge speed (25 ns). Our results provide a simple and novel way to design high-performance $AgNbO_3$-based energy storage lead-free ceramics.

Handling Editor: David Cann.

Tianyu Li, Wenjun Cao and Pengfei Chen contributed equally to this work.

Address correspondence to E-mail: ccwang@ahu.edu.cn

https://doi.org/10.1007/s10853-021-06148-x

GRAPHICAL ABSTRACT

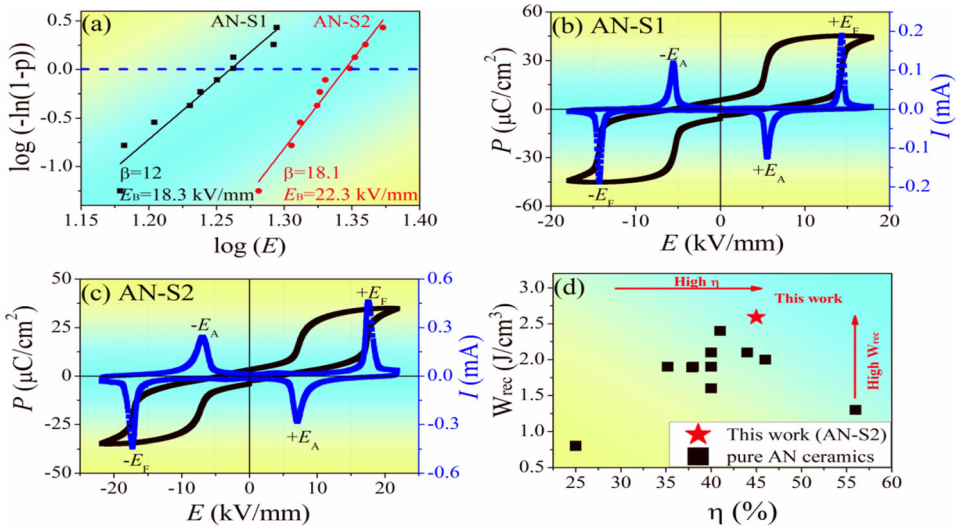

Introduction

Compared with traditional electricity energy storage devices, such as lithium batteries, and supercapacitors, dielectric ceramic capacitors are characterized by high power density and ultrafast charge/discharge rates, and treated as crucial factors for pulsed power systems [1–4]. The evaluations of recoverable energy storage density (W_{rec}) and energy storage efficiency (η) are based on the polarization–electric field (P–E) hysteresis loop [3]:

$$W_{rec} = \int_{Pr}^{Pmax} EdP \quad (1)$$

$$\eta = \frac{W_{rec}}{W_{rec} + W_{loss}} \quad (2)$$

where E is the applied electric field, P_{max} is the saturated polarization, P_r is the remnant polarization, and W_{loss} is the energy loss density, which equals to the area surrounded by the hysteresis loop. From Eq. (1), we can clear see that to achieve high W_{rec}, dielectric energy storage materials must have both large ΔP (P_{max}-P_r) value and high breakdown electric field strength (E_B). Among a large number of dielectric energy storage ceramics, antiferroelectric (AFE) ceramics owing to their double polarization hysteresis loops show large ΔP (P_{max}-P_r) (high P_{max} and low P_r) and W_{rec} values [5–12]. Unfortunately, most of the AFE ceramics for energy storage application contain lead element [5–10], which is harmful for human health and environment. Therefore, the development of new lead-free AFE energy storage ceramics is extremely urgent.

In 2016, Zhao et al. reported that pure $AgNbO_3$ lead-free ceramics showed typical double P–E loops (antiferroelectric behavior) and a high W_{rec} of 1.6 J/cm^3 at 14 kV/mm [13]. This finding has triggered a burst of research activities on $AgNbO_3$ ceramics [12–19]. So far, the effective method to further enhance W_{rec} of $AgNbO_3$ ceramics is A- or B-site elements doping. For example, Zhao et al. found that Ta_2O_5 modified in $AgNbO_3$ led to the E_B value increasing from 17 to 24 kV/mm, and an ultrahigh W_{rec} value of 4.2 J/cm^3 was obtained in $AgNb_{0.85}Ta_{0.15}O_3$ ceramic [12]. In addition, Luo et al. also reported that $Ag_{0.91}Sm_{0.03}NbO_3$ (ASN) sample showed excellent energy storage performances of W_{rec} = 5.2 J/cm^3 and η = 68.5% [14].

It is generally known that sintering method has an important effect on the structural and electrical

properties of ceramics [20–22]. In 2000, Chen and Wang et al. proposed a novel, low cost and extremely simple sintering technology, named as two-step sintering method [23]. A number of studies have confirmed that two-step sintering method can improve electrical properties of ceramics by increasing the density and suppressing grain growth [20, 23–26]. Additionally, the low dwelling temperature in two-step sintering method can effectively reduce the volatilization of elements with lower melting point, such as Na, Bi, K elements [20, 22, 26]. The currently reported sintering temperature of $AgNbO_3$ ceramics is mostly between 1050 and 1150 °C [12–19]. However, the melting point temperature of Ag element (961 °C) is much lower than the sintering temperature of the $AgNbO_3$ ceramics. This will inevitably cause the volatilization of Ag element, thus forming the defects such as Ag vacancies ($V_{Ag}^{'}$ *s*) which, in turn, create oxygen vacancies ($V_O^{\bullet\bullet}$ *s*) to maintain electrical neutrality. Defect dipole such as $V_{Ag}^{'} - v_O^{\bullet\bullet} - V_{Ag}^{'}$, therefore, is formed in $AgNbO_3$ ceramics. Moriwake et al. [27] using first principles calculations found that the presence of defect dipole $V_{Ag}^{'} - v_O^{\bullet\bullet} - V_{Ag}^{'}$ in $AgNbO_3$ could also lead to weak ferroelectricity in the *Pbcm* phase, which would reduce the energy storage efficiency (η) of the ceramic [19]. Therefore, it can be seen that controlling the volatilization of Ag element is very important to improve the energy storage characteristics of $AgNbO_3$ ceramics.

In this work, we present a comparative study on the energy storage performances of $AgNbO_3$ ceramics prepared by the traditional single-step sintering method and the two-step sintering method. Our results indicate that the sample prepared by the two-step sintering method exhibits high breakdown electric field strength (22 kV/mm), larger W_{rec} (2.59 J/cm^3) and higher η (45%). These values not only are superior to those in the sample prepared by single-step sintering method, but also rival those reported in pure $AgNbO_3$ ceramics [13, 16, 18, 21, 28–34].

Experimental procedure

All the $AgNbO_3$ ceramics were prepared by traditional solid-state reaction method using high purity raw materials of Ag_2O (99.7%) and Nb_2O_5 (99.99%). These raw materials were precisely weighed accordingly the corresponding stoichiometry and then ball milled at 300 rpm for 24 h. The milled powders were calcined at 870 °C for 6 h in O_2 atmosphere. After that, the calcined powders were ball milled again for 12 h. The resultant powders were pressed into pellets of 14 mm in diameter and 1 mm in thickness under uniaxial pressure of 80 MPa using PVA as binder. After removing the PVA binder, the pellets by single-step sintering method were sintered at 1080 °C for 6 h in O_2 atmosphere, and named as AN-S1. For comparison, the pellets by two-step sintering method were heated at 1100 °C without heat preservation, then cooled down directly to 950 °C for 10 h in air and then cool down to room temperature. After that, the sintered samples were annealed at 950 °C for 4 h in O_2 atmosphere, and named as AN-S2. Notably, all the pellets are covered with powders of the same composition to reduce the volatilization of Ag element during the sintering process. It should be noted that the samples for measuring energy storage properties were polished to achieve parallel and smooth faces with thickness of ~0.2 mm and coated on both sides with Au electrodes with diameter of 2 mm. In addition, the power density of the ceramic samples was tested by a charge–discharge platform (Gogo Instruments Technology, Shanghai, China). The details of structural and electrical properties can be found in our previous work [35, 36].

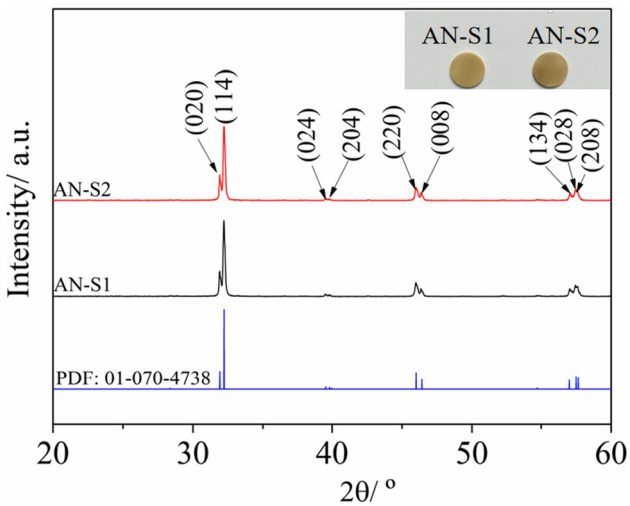

Figure 1 XRD patterns of the AN S1 and S2. The inset is the photograph images of the samples.

Results and discussion

XRD patterns of the AN-S1 and S2 are indicated in Fig. 1. Both samples exhibit pure perovskite structure without no secondary phases. As shown in the inset of Fig. 1, the color of both samples is yellow. These results suggest that the AN-S1 and S2 show good crystallinity. The SEM images obtained from polished and thermally etched surface of AN-S1 and S2 are displayed in Fig. 2 a and b, respectively. It can be clearly seen that both of them show dense microstructure. The relative density (ρ_r) of AN-S2 sample was deduced by Archimedes method and found to be 97% of the theoretical value, which is more than 93% of AN-S1. Additionally, the AN-S2 sample also exhibits smaller grain size and homogeneous microstructure as indicated from Fig. 2 a and b and Fig. S1 of the supplementary materials. Both facts are helpful for energy storage. The element mappings performed on the AN-S2 ceramic are present in Fig. S2(a–c). It is seen that all the elements in the ceramic are homogeneously distributed.

The temperature dependence of dielectric constant and loss tangent measured at various frequencies for the AN-S1 and S2 is presented in Fig. 3. A number of dielectric anomalies, signaling a series of phase transitions, have been observed in both samples. From low to high temperature, the first dielectric anomaly occurs at about 60 °C, relating to M1 ($Pmc2_1$)–M2 (*Pbcm*) phase transitions. The next dielectric anomaly observed at around 250 °C associated with M2 (*Pbcm*)–M3 (*Pbcm*) transition. Finally, a sharply increased dielectric constant is found around 340 °C, corresponding to the M3-O phase transition [28]. Details of the phase transition temperatures for both the samples are summarized in Table 1. It is worth noting that the dielectric loss tangent of AN-S2 sample is significantly smaller than that of AN-S1. In order to show that the AN-S2 sample has a smaller dielectric loss value, the inset shows the dielectric loss at −25 ∼ 50 °C of both samples. As a result, the dielectric loss value of AN-S2 sample (tanδ = 0.0186 @25 °C 1 kHz) is indeed smaller than that of AN-S1 sample (tanδ = 0.0209 @25 °C 1 kHz). The reason for this finding may be that the two-step sintering method can effectively reduce the volatilization of Ag element, thereby reducing the oxygen vacancy concentration in the sample. In order to verify the above point, XPS measurements (0.1 s) are conducted on both AN ceramics, as shown in Fig. S3 of the supplementary materials. It is clearly shown that the 0.1 s spectrum can be fitted by two Gaussian peaks; from low to high binding energy, the peak corresponds successively to oxygen atoms at the lattice site and oxygen vacancies, which is similar to previously reported results [19]. Moreover, the oxygen vacancy concentration in AN-S2 sample (22.5%) is smaller than AN-S1 (29.2%). This result also better illustrates that the two-step sintering method can reduce the generation of oxygen vacancies by controlling the volatilization of Ag element. The low dielectric loss tangent value is an important factor for sample with high energy storage ability. Therefore, an enhanced energy storage performance would be expected in AN-S2.

In order to well study the feasibility for practical dielectric energy storage applications, the Weibull distribution analysis plots of the E_B values for the AN-S1 and S2 are given in Fig. 4a. It can be seen that the data were well fitted linearly, and high β values suggested the reliability of the Weibull analysis. Importantly, we can also observe that the average E_B value of AN-S2 sample is much higher than that of AN-S1 sample, indicating that the AN-S2 sample can

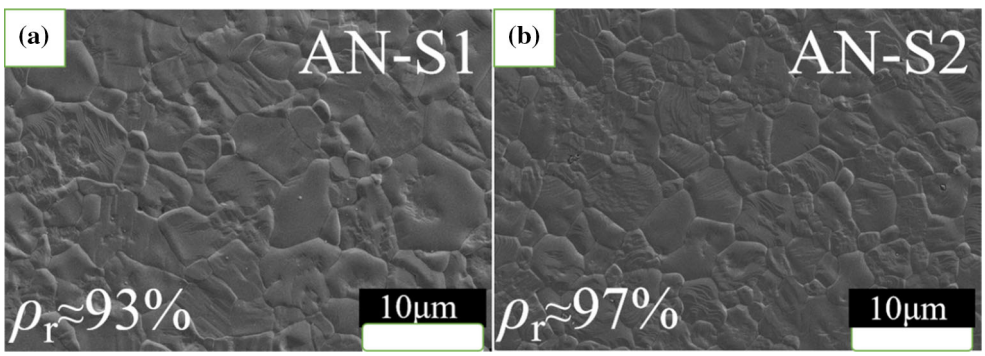

Figure 2 **a** and **b** SEM images of the AN S1 and S2.

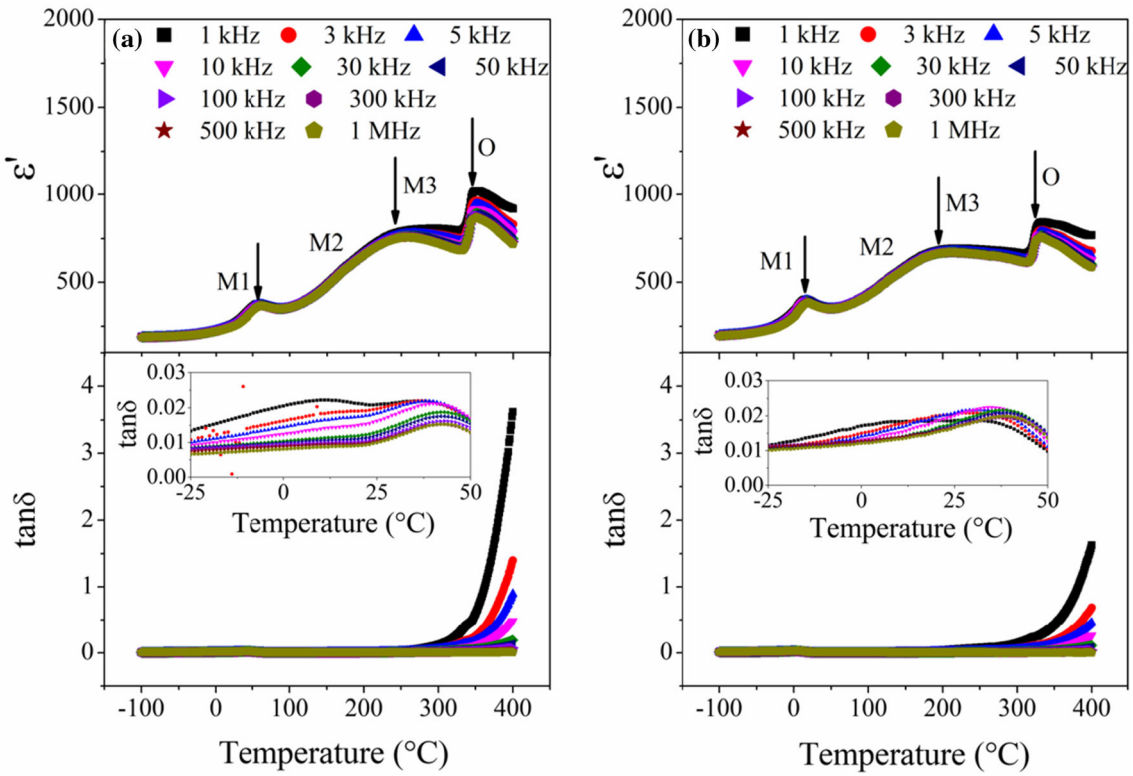

Figure 3 Temperature dependence of dielectric constant and loss tangent measured at various frequencies for AN-S1 **(a)** and AN-S2 **(b)**.The inset shows the dielectric loss at −25–50 °C.

Table 1 Dielectric and energy storage characteristic parameters of the AN-S1 and AN-S2 samples

Sample	M1–M2 (°C)	M2–M3 (°C)	M3–O (°C)	W_{rec} (J/cm^3)	η(%)
AN-S1	61	243	350	2.21	35
AN-S2	54	238	333	2.59	45

be operated at much higher electric field with an enhanced W_{rec} value. In general, the breakdown field strength is closely related to the ceramics microstructure features [3], such as grain size, density, secondary phase and so on. Among them, the grain size and density have strong effect on the breakdown field strength of dielectric ceramics; that is, small grain size, homogeneous and dense microstructure can significantly improve the dielectric breakdown strength [3]. Therefore, it is reasonable to believe that the high breakdown field strength of AN-S2 samples is related to their smaller grain size and higher density. Furthermore, Fig. 4b and c shows *P*–*E* and *I*–*E* loops of the AN-S1 and AN-S2 ceramics measured at room temperature. Typical antiferroelectric double *P*–*E* loops are observed in both samples. Moreover, four current peaks are seen in the *I*–*E* loops in both samples, with two peaks in both forward and backward branches. In each branch, the peak at higher electric field is related to the antiferroelectric-ferroelectric phase transition [37] (marked as E_F), while another peak at lower electric field is associated to the ferroelectric-antiferroelectric phase transition [37] (marked as E_A). In addition, based on Eqs. (1) and (2), the calculated W_{rec} and η values for both samples are present in Table 1. It should be noted that both the W_{rec} and η values of AN-S2 are much higher than those of AN-S1. These results suggest that two-step sintering method significantly enhances the energy storage properties of the $AgNbO_3$ ceramics. To better verify this view, Fig. 4d comparisons of the $\eta \sim W_{rec}$ of the AN-S2 ceramic prepared by two-step sintering method studied in this work with pure $AgNbO_3$ ceramics reported in published literature [13, 16, 18, 21, 28–34]. It is

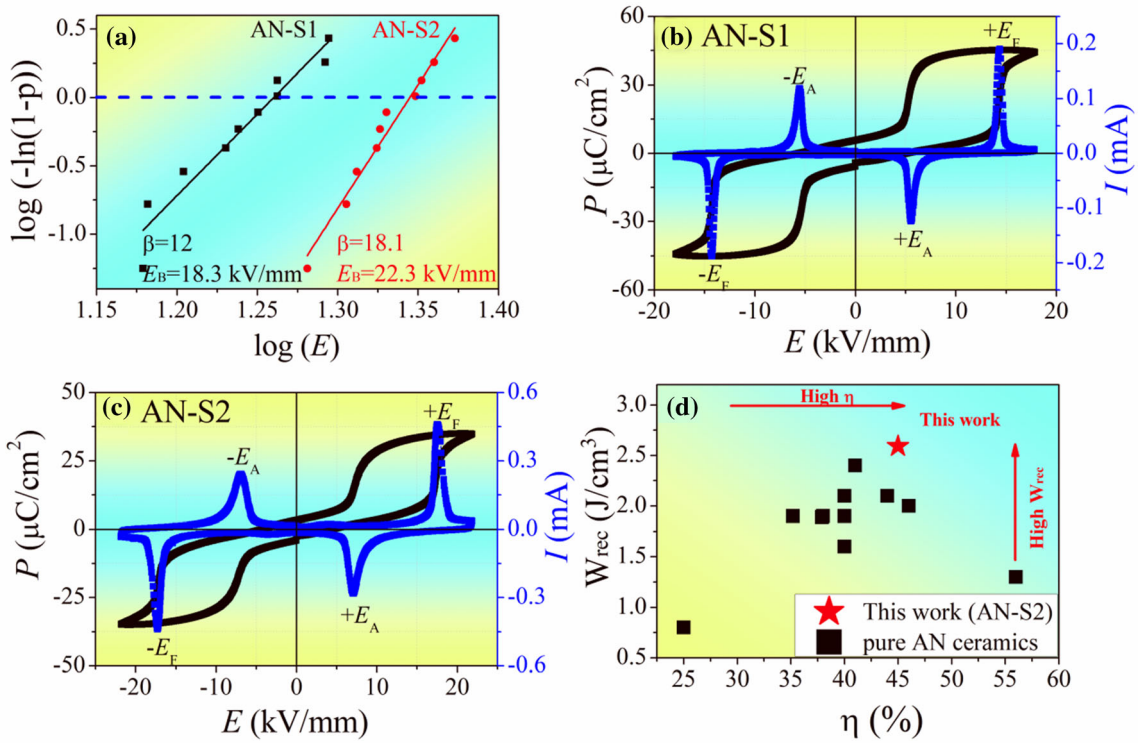

Figure 4 Weibull plots of the EB values for AN-S1 and -S2 ceramics **(a)**,P-E and I-E loops measured at room temperature for AN-S1 **(b)** and AN-S2 **(c)** and comparison of Wrec and η of the AN-S2 studied in this work with pure AgNbO3 (AN) ceramics published in literature **(d)**.

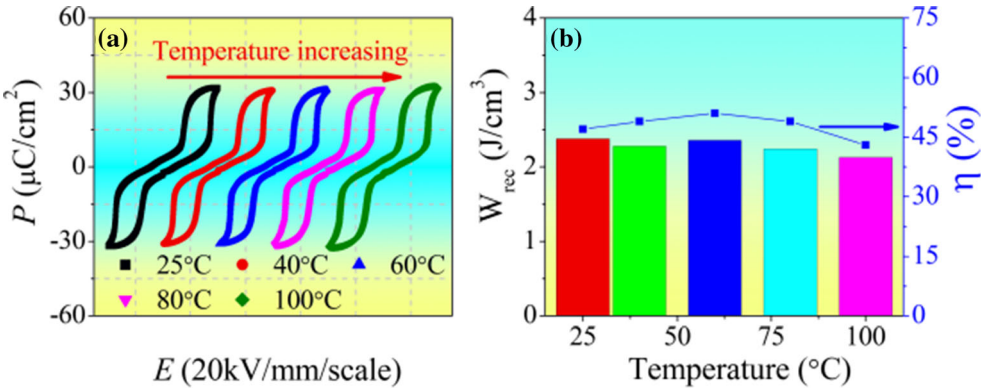

Figure 5 **a** P-E loops of the AN-S2 ceramic measured at 20 kV/mm and 10 Hz in the temperature range of 25–100 °C, **b** Wrec and η values as a function of temperature.

obvious that the energy storage properties of the AN-S2 ceramic are superior to all of them.

Figure 5a shows *P*–*E* loops of the AN-S2 ceramic measured at 20 kV/mm and 10 Hz in the temperature range of 25–100 °C. It can be found that the double *P*–*E* loops can be seen in the temperature range. Moreover, the calculated W_{rec} and η values are presented in Fig. 5b; the W_{rec} values firstly slightly increased to 2.39 J/cm^3, and then decreased to 2.13 J/cm^3 at 100 °C. In general, the thermal stability of energy storage density can be calculated according to equation [36, 38]:

$$\frac{\Delta W}{W_{25^\circ C}} = \frac{W - W_{25^\circ C}}{W_{25^\circ C}} \times 100\% \quad (3)$$

where ΔW and $W_{25^\circ C}$ are the variation of energy storage density and the value of energy storage density measured at 25 °C, respectively. The

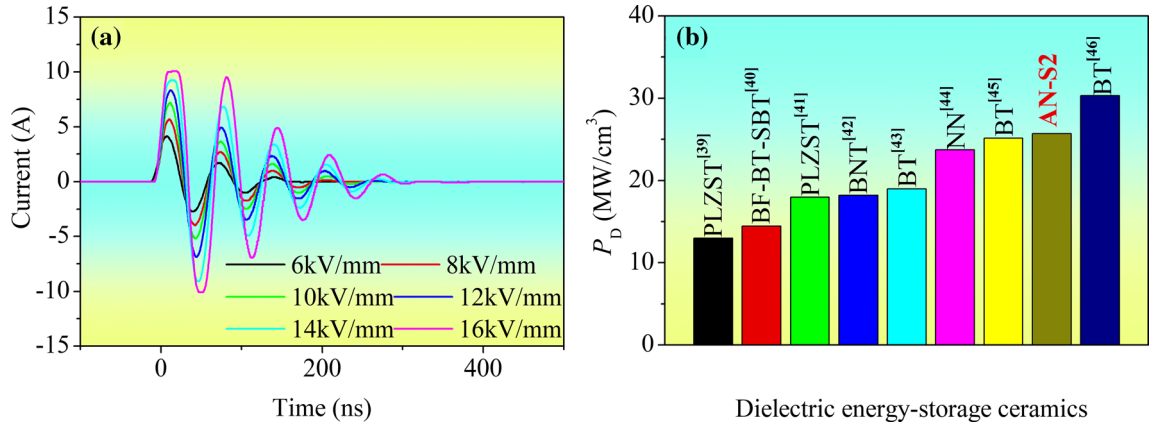

Figure 6 **a** Undamped pulsed discharge current curves of AN-S2 ceramic measured at room temperature and various electric fields, and **b** comparison of the power density (PD) of the AN-S2 ceramic studied in this work with other dielectric energy storage ceramics from published literature.

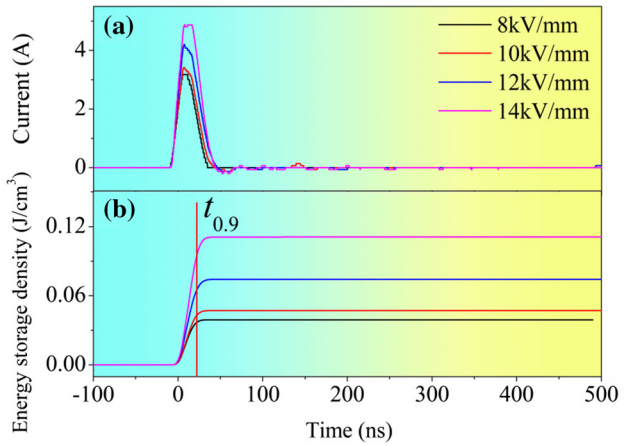

Figure 7 **a** Damped pulsed discharge current curves, and **b** energy storage density and discharge versus time of AN-S2 ceramic measured at room temperature and various electric fields.

corresponding thermal stability of energy storage density is lower than 10% in the temperature range of 25–100 °C. What is more, the η values of 43–52% can also be kept in the wide temperature range.

In order to systematically characterize the energy storage characteristics of AN-S2 samples, the undamped and damped discharge current curves are presented in Figs. 6 and 7, respectively. From Fig. 6a, it can be seen that the current peaks increase from 4.13 to 10.08 A as the applied electric field increases from 6 to 16 kV/mm. The power density (P_D) can be calculated as the below formula:

$$P_D = EI_{max}/2S \quad (4)$$

where E is the applied electric field, I_{max} is the value of current peak, and S is the electrode area. A high power density (P_D) value of 25.7 MW/cm^3 is achieved in the AN-S2 sample. It is worth noting that the P_D value of AN-S2 sample is higher than most of the reported values so far in different energy storage materials [39–46] as compared in Fig. 6b. Furthermore, the damped discharge current curves show that the value of current peak increases from 3.17 to 4.87 A as the electric field increases from 8 to 14 kV/mm (as seen in Fig. 7a). It is well known that the energy storage density in the discharge processes can be calculated as follows:

$$W_{Discharge} = \frac{R\int i(t)^2 dt}{V} \quad (5)$$

where R is the total resistance (for this work, it is 130 Ω), V is the total volume of the ceramic, i is the current, and t stands for the time. The evolution of energy storage density in the discharge process as a function of electric field is shown in Fig. 7b as well. The results reveal that the energy storage density gradually increases from 0.04 to 0.1 J/cm^3 when the electric field increases from 8 to 14 kV/mm. On the other side, it is generally named the $t_{0.9}$—the time of 90% of the total energy has been discharged as the discharging time in dielectric energy materials [35, 45, 47, 48], as also shown by the vertical line in Fig. 7b. And the $t_{0.9}$ measured at room temperature is around 25 ns at 14 kV/mm, which suggests that the discharge speed is extremely fast in the AN-S2 ceramic.

Conclusions

In this study, the pure $AgNbO_3$ lead-free antiferroelectric ceramic with improved energy storage properties was prepared by two-step sintering method. The ceramic prepared by two-step sintering method exhibited high breakdown electric field strength (22 kV/mm), large W_{rec} (2.59 J/cm^3) and high η (45%) as well as excellent temperature stability. The main reason for above excellent energy storage characteristics may due to the ceramic prepared by the two-step sintering method has small grain size, dense and homogeneous microstructure. Furthermore, it also exhibited high power density (P_D = 25.7 MW/cm^3) and extremely fast charge–discharge speed (25 ns).

Acknowledgements

The authors acknowledge financial support from the National Natural Science Foundation of China (Grant Nos. 51872001 and 51572001). This work was supported in part by the Open Research Fund Program of the State Key Laboratory of Low-Dimensional Quantum Physics (Grant No. KF201803).

Declarations

Conflict of interest The authors declare that they have no conflict of interest.

Supplementary Information: The online version contains supplementary material available at https://doi.org/10.1007/s10853-021-06148-x.

References

[1] Chu BJ, Zhou X, Ren KL, Neese B, Lin MR, Wang Q, Bauer F, Zhang QM (2006) A dielectric polymer with high electric energy density and fast discharge speed. Science 313:334–336

[2] Pan H, Li F, Liu Y, Zhang QH, Wang M, Lan S, Zheng YP, Ma J, Gu L, Shen Y, Yu P, Zhang SJ, Chen LQ, Lin YH, Nan CW (2019) Ultrahigh-energy density lead-free dielectric films via polymorphic nanodomain design. Science 365:578–582

[3] Yang LT, Kong X, Li F, Hao H, Cheng ZX, Liu HX, Li JF, Zhang SJ (2019) Perovskite lead-free dielectrics for energy storage applications. Prog Mater Sci 102:72–108

[4] Hao XH, Zhai JW, Kong LB, Xu ZK (2014) A comprehensive review on the progress of lead zirconate-based antiferroelectric materials. Prog Mater Sci 63:1–57

[5] Yang Y, Liu P, Zhang YJ, Kandula KR, Xu JW, Zhang GZ, Jiang SL (2020) Low electric-field-induced strain and high energy storage efficiency in (Pb, Ba, La)(Zr, Sn, Ti)O_3 antiferroelectric ceramics through regulating the content of La. Ceram Int 46:18106–18113

[6] Huang KW, Ge GL, Yan F, Shen B, Zhai JW (2020) Ultralow electrical hysteresis along with high energy-storage density in lead-based antiferroelectric ceramics. Adv Electron Mater 6:1901366

[7] Li L, Wang RX, Gu ZB, Lu MH, Zhu MW, Zhang ST (2020) Energy storage property of $(Pb_{0.97}La_{0.02})(Zr_{0.5}Sn_{0.4}Ti_{0.1})O_3$-$(Na_{0.5}Bi_{0.5})_{0.94}Ba_{0.06}TiO_3$ ceramics: effects of antiferroelectric-relaxor transition and improved breakdown strength. J Eur Ceram Soc 40:2996–3002

[8] Qiao PX, Chen XF, Liu Z, Wang GS, Dong XL (2020) Enhanced energy storage performance in $Pb_{0.97}La_{0.02}(Zr_x$-$Sn_{0.90-x}Ti_{0.10})O_3$ antiferroelectric ceramics. Mater Lett 260:126877

[9] Liu XH, Li Y, Sun NN, Hao XH (2020) High energy-storage performance of PLZS antiferroelectric multilayer ceramic capacitors. Inorg Chem Front 7:756–764

[10] Liu Z, Chen XF, Peng W, Xu CH, Dong XL, Cao F, Wang GS (2015) Temperature-dependent stability of energy storage properties of $Pb_{0.97}La_{0.02}(Zr_{0.58}Sn_{0.335}Ti_{0.085})O_3$ antiferroelectric ceramics for pulse power capacitors. Appl. Phys. Lett. 106:262901

[11] Li QN, Zhou CR, Xu JW, Yang L, Zhang X, Zeng WD, Yuan CL, Chen GH, Rao GH (2016) Tailoring antiferroelectricity with high energy-storage properties in Bi0.5Na0.5TiO3-BaTiO3 ceramics by modulating Bi/Na ratio. J Mater Sci: Mater Electron 27:10810–10815

[12] Zhao L, Liu Q, Gao J, Zhang SJ, Zhang JF (2017) Lead-free antiferroelectric sliver niobate tantalate with high energy storage performance. Adv Mater 29:1701824

[13] Zhao L, Liu Q, Zhang SJ, Li JF (2016) Lead-free $AgNbO_3$ anti-ferroelectric ceramics with an enhanced energy storage performance using MnO_2 modification. J Mater Chem C 4:8380–8384

[14] Luo NN, Han K, Zhuo FP, Xu C, Zhang GZ, Liu LJ, Chen XY, Hu CZ, Zhou HF, Wei YZ (2019) Aliovalent A-site engineered $AgNbO_3$ lead-free antiferroelectric ceramics toward superior energy storage density. J Mater Chem A 7:14118–14128

[15] Gao J, Zhang YC, Zhao L, Li KY, Liu Q, Studer A, Hinterstein M, Zhang SJ, Li JF (2019) Enhanced antiferroelectric phase stability in La-doped $AgNbO_3$: perspectives from

the microstructure to energy storage properties. J Mater Chem A 7:2225–2232

[16] Xu YH, Guo Y, Liu Q, Yin YH, Bai JL, Lin L, Tian JJ, Tian Y (2020) Enhanced energy density in Mn-doped (1–x)AgNbO3-xCaTiO3 lead-free antiferroelectric ceramics. J Alloys Compd 821:153260

[17] Tian Y, Jin L, Zhang HF, Xu Z, Wei XY, Viola G, Abrahams I, Yan HX (2017) Phase transitions in bismuth-modified silver niobate ceramics for high power energy storage. J Mater Chem A 5:17525–17531

[18] Yan ZN, Zhang D, Zhou XF, Qi H, Luo H, Zhou KC, Abrahams I, Yan HX (2019) Silver niobate based lead-free ceramics with high energy storage density. J Mater Chem A 7:10702–10711

[19] Luo NN, Han K, Zhuo FP, Liu LJ, Chen XN, Peng BL, Wang XP, Feng Q, Wei YZ (2019) Design for high energy storage density and temperature-insensitive lead-free antiferroelectric ceramics. J Mater Chem C 7:4999–5008

[20] Ye G, Wade-Zhu J, Zou J, Zhang T, Button TW, Binner J (2020) Microstructure, piezoelectric properties and energy harvesting performance of undoped $(K_{0.5}Na_{0.5})NbO_3$ lead-free ceramics fabricated via two-step sintering. J Eur Ceram Soc 40:2977–2988

[21] Ren PR, Ren D, Sun L, Yan FX, Yang S, Zhao GY (2020) Grain size tailoring and enhanced energy storage properties of two-step sintered Nd^{3+}-doped $AgNbO_3$. J Eur Ceram Soc 40:4495–4502

[22] Ding JX, Liu YF, Lu YN, Qian H, Gao H, Chen H, Ma CJ (2014) Enhanced energy-storage properties of $0.89Bi_{0.5}Na_{0.5}TiO_3$-$0.06BaTiO_3$-$0.05K_{0.5}Na_{0.5}NbO_3$ lead-free antiferroelectric ceramics by two-step sintering method. Mater Lett 114:107–110

[23] Chen I-We, Wang X-H (2000) Sintering dense nanocrystalline ceramics without final-stage grain growth. Nature 404:168

[24] Wang XH, Deng XY, Bai HL, Zhou H, Qu WG, Li LT, Chen IW (2006) Two-step sintering of ceramics with constant grain-size, II: $BaTiO_3$ and Ni-Cu-Zn ferrite. J Am Ceram Soc 89:438–443

[25] Fathi MH, Kharaziha M (2009) Two-step sintering of dense, nanostructural forsterite. Mater Lett 63:1455–1458

[26] Wang C, Fang BJ, Qu YH, Chen ZH, Zhang S, Ding JN (2020) Preparation of KNN based lead-free piezoelectric ceramics via composition designing and two-step sintering. J Alloys Compd 832:153043

[27] Moriwake H, Fisher CAJ, Kuwabara A, Fu DS (2013) First-principles study of point defect formation in $AgNbO_3$. Jpn J Appl Phys 52:09KF08

[28] Gao J, Zhao L, Liu Q, Wang XP, Zhang SJ, Li JF (2018) Antiferroelectric-ferroelectric phase transition in lead-free $AgNbO_3$ ceramics for energy storage applications. J Am Ceram Soc 101:5443–5450

[29] Tian Y, Jin L, Zhang HF, Xu Z, Wei XY, Politova ED, Stefanovich SY, Tarakina NV, Abrahams I, Yan HX (2016) High energy storage density in sliver niobate ceramics. J Mater Chem A 4:17279–17287

[30] Han K, Luo NN, Miao SF, Zhuo FP, Chen XY, Liu LJ, Hu CZ, Zhou HF, Zhou HF, Wang XP, Wei YZ (2019) Realizing high low-electric-field energy storage performance in $AgNbO_3$ ceramics by introducing relaxor behaviour. J Materiomics 5:597–605

[31] Luo NN, Han K, Liu LJ, Peng BL, Wang XP, Hu CZ, Zhou HF, Feng Q, Chen XY, Wei YZ (2019) Lead-free $Ag_{1-3x}La_xNbO_3$ antiferroelectric ceramics with high energy storage density and efficiency. J Am Ceram Soc 102:4640–4647

[32] Xu CH, Fu ZQ, Liu Z, Wang L, Yan SG, Chen XF, Cao F, Dong XL, Wang GS (2018) La/Mn codoped $AgNbO_3$ lead-free antiferroelectric ceramics with large energy density and power density, ACS sustain. Chem Eng 6:16151–16159

[33] Mao SF, Luo NN, Han K, Feng Q, Chen XY, Peng BL, Liu LJ, Hu CZ, Zhou HF, Toyohisa F, Wei YZ (2020) Effect of Lu doping on the structure, electrical properties and energy storage performance of $AgNbO_3$ antiferroelectric ceramics. J. Mater. Sci: Mater Electron 31:7731–7741

[34] Ma JL, Yan SG, Xu CH, Cheng GF, Mao CL, Bian JJ, Wang GS (2019) Enhanced energy storage properties of silver niobate ceramics under hydrostatic pressure. Mater Lett 247:40–43

[35] Li TY, Chen PF, Li F, Wang CC (2021) Energy storage performance of $Na_{0.5}Bi_{0.5}TiO_3$-$SrTiO_3$ lead-free relaxors modified by $AgNb_{0.85}Ta_{0.15}O_3$. Chem. Eng. J. 406:127151

[36] Li TY, Chen PF, Si RJ, Li F, Guo YM, Wang CC (2020) High energy storage density and efficiency with excellent temperature and frequency stabilities under low operating field achieved in $Ag_{0.91}Sm_{0.03}NbO_3$-modified $Na_{0.5}Bi_{0.5}TiO_3$-$BaTiO_3$ ceramics. J Mater Sci: Mater Electron 31:6928–16937

[37] Han K, Luo NN, Jing Y, Wang XP, Peng BL, Liu LJ, Hu CZ, Zhou HF, Wei YZ, Chen XY, Feng Q (2019) Structure and energy storage performance of Ba-modified $AgNbO_3$ lead-free antiferroelectric ceramics. Ceram Int 45:5559–5565

[38] Liu ZC, Ren PR, Wang LCB, X, Wan YH, Zhao GY, (2017) Enhanced energy storage properties of $NaNbO_3$ and $SrZrO_3$ modified $Bi_{0.5}Na_{0.5}TiO_3$ based ceramics. J Alloys Compd 721:538–544

[39] Xu R, Tian JJ, Zhu QS, Zhao T, Feng YJW, XY, Xu Z, (2017) Effects of La-induced phase transition on energy storage and discharge properties of PLZST ferroelectric/antiferroelectric ceramics. Ceram Int 43:13918–13923

[40] Chen ZT, Bu XY, Ruan BX, Du J, Zheng P, Li LL, Wen F, Bai WF, Wu W, Zheng L, Zhang Y (2020) Simultaneously achieving high energy storage density and efficiency under low electric field in $BiFeO_3$-based lead-free relaxor ferroelectric ceramics. J Eur Ceram Soc 40:5450–5457

[41] Xu CH, Liu Z, Chen XF, Yan SG, Cao F, Dong XL, Wang GS (2016) High charge-discharge performance of $Pb_{0.98}La_{0.02}(Zr_{0.35}Sn_{0.55}Ti_{0.10})_{0.995}O_3$ antiferroelectric ceramics. J. Appl. Phys. 120:074107

[42] Li F, Yang K, Liu X, Zou J, Zhai JW, Shen B, Li P, Shen J, Liu BH, Chen P, Zhao KY, Zeng HR (2017) Temperature induced high charge–discharge performances in lead–free $Bi_{0.5}Na_{0.5}TiO_3$–based ergodic relaxor ferroelectric ceramics. Scripta Mater 141:15–19

[43] Shi F, Tang B, Fang ZX, Li H, Zhang SR (2019) Enhanced energy storage and fast charge-discharge properties of $(1–x)BaTiO_3$-$xBi(Ni_{1/2}Sn_{1/2})O_3$ relaxor ferroelectric ceramics. Ceram Int 45:17580–17590

[44] Zhou MX, Liang RH, Zhou ZY, Yan SG, Dong XL (2018) Novel sodium niobate-based lead-free ceramics as new environment-friendly energy storage materials with high energy density, high power density, and excellent stability. ACS Sustain Chem Eng 6:12755–12765

[45] Liu G, Li Y, Shi MQ, Yu LJ, Chen P, Yu K, Yan Y, Jin L, Wang DW, Gao JH (2019) An investigation of the dielectric energy storage performance of $Bi(Mg_{2/3}Nb_{1/3})O_3$-modified $BaTiO_3$ Pb-free bulk ceramics with improved temperature/frequency stability. Ceram Int 45:19189–19196

[46] Zhou MX, Liang RH, Zhou ZY, Dong XL (2018) Novel $BaTiO_3$-based lead-free ceramic capacitors featuring high energy storage density, high power density, and excellent stability. J Mater Chem C 6:8528–8537

[47] Wang JH, Li Y, Sun NN, Du JH, Zhang QW, Hao XH (2019) $Bi(Mg_{0.5}Ti_{0.5})O_3$ addition induced high recoverable energy-storage density and excellent electrical properties in lead-free $Na_{0.5}Bi_{0.5}TiO_3$-based thick films. J Eur Ceram Soc 40:255–263

[48] Liu JR, Yang K, Zhai JW, Shen B, Wang HT, Li F (2018) High energy storage density and rapid discharge speed of niobosilicate glasses. Mater Chem Phys 206:29–34